Targeting the translation machinery: The RNase Y specificity factor Y-complex coordinates ribosome degradation

Fabián A. Cornejo[1,*], Kristina Driller[1,2,*], Rina Ahmed-Begrich[1], Katja Schmidt[1], Michael Jahn[1], Vivekanandan Shanmuganathan[1], Karin Hahnke[1], Florian Kondrot[1], Thomas F. Wulff[1], Sebastian Rämisch[1], Kathirvel Alagesan[1], Emmanuelle Charpentier[1,3], and Kürşad Turgay[1,2]

[1]Max Planck Unit for the Science of Pathogens, Berlin, Germany

[2]Leibniz Universität Hannover, Institute of Microbiology, Hannover, Germany

[3]Humboldt-Universität zu Berlin, Institute of Biology, Berlin, Germany

* These authors equally contributed to this work

Correspondence to: cornejo@mpusp.mpg.de, turgay@mpusp.mpg.de

Abstract

Limiting the synthesis and activity of ribosomes is crucial for responding to various stresses, including nutrient starvation or proteotoxic stress. In *Bacillus subtilis,* this can be achieved through the coordinated action of the alarmones (p)ppGpp and the transcription factor Spx. In this study, we performed a genetic screen to identify new factors involved in the heat shock response of *B. subtilis*. We discovered that the RNase Y specificity factor Y-complex plays an important role in the heat shock response and the transition to the stationary growth phase. The Y-complex is required for the processing of various RNAs, including the maturation of mRNAs encoding proteins involved in translation and metabolism. We further demonstrate that the Y-complex and RNase Y initiate the degradation of rRNAs in mature ribosomes, lowering their abundance. We propose the Y-complex as a system by which *B. subtilis* regulates protein synthesis and resource allocation after exponential growth.

Keywords: *Bacillus subtilis*, Ribosome, Stress response, Y-complex, RNase Y, Ribosome degradation, Heat shock, (p)ppGpp

Introduction

Bacteria can sense, adapt to, and survive stressful environmental changes facilitated by various general and specific stress response systems. Proteotoxic stresses, like high temperatures, significantly disrupt protein folding and can lead to the formation of toxic protein aggregates. Chaperones and proteases are expressed as a response due to the inactivation of the transcriptional repressors HrcA and CtsR in *Bacillus subtilis*[1–4]. The activation of the protein quality control (PQC) allows the refolding of un- or misfolded proteins by different chaperone systems or the degradation of irreparable proteins through AAA+ protease complexes like ClpCP[5,6].

In addition to the repairing or removal of protein aggregates, inhibiting translation is crucial for survival during proteotoxic stresses, as it can alleviate the extra load on the PQC system[7–10]. In *Bacillus subtilis*, the nucleotide second messengers guanosine tetraphosphate and guanosine pentaphosphate, collectively referred to as (p)ppGpp, and the transcription factor Spx independently regulate synthesis and activity of ribosomes during stress[7,11]. Spx is a redox-sensitive heat shock transcription factor that controls the expression of redox chaperones and simultaneously represses transcription of translation-related genes during oxidative and heat shock response[11–14].

The alarmones (p)ppGpp were initially discovered to be synthesized during amino acid starvation, but more recently, it was observed that their synthesis is also induced by protein folding stresses, such as heat or oxidative stress[7]. During heat stress, their accumulation results in increased thermoresistance, inhibition of translation, and a reduction in protein aggregation[7]. (p)ppGpp inhibit translation by binding to specific GTPases (e.g. IF2, RbgA)[15–17]. Furthermore, (p)ppGpp accumulation can lead to decreased transcription of e.g. rRNA and ribosomal protein (r-protein) transcripts by inhibiting GTP biosynthesis and reducing its levels[18,19]. This downregulation of translation is an important component of the response to nutrient scarcity as well as heat shock.

In this study, we aimed to identify new genes or pathways involved in the heat shock response using a genetic screen that reports on fitness. We identified that the Y-complex (RicAFT-complex), which interacts with the endonuclease RNase Y and conveys substrate specificity, plays a role in the heat shock response. We demonstrate further that the Y-complex regulates ribosome levels by initiating ribosome degradation during nutrient depletion or heat shock. Mutants lacking a Y-complex member show increased ribosome levels before and during heat shock, increasing the burden on the PQC system and, in consequence, protein aggregation during heat stress. These findings not only indicate the importance of RNases during stress response but also emphasize that controlling the stability of RNA is an important general mechanism to modify cellular function.

Results

The Y-complex is necessary for survival during heat shock

To identify genes that play a role in the heat shock response, we used the BKE single-mutant library[20], which includes a barcoded deletion cassette for each non-essential gene in *B. subtilis*. All gene deletion mutant strains were pooled, grown at 30°C, and subjected to a mild heat shock at 50°C during the mid-exponential phase, while a control was maintained at 30°C. Relative fitness scores for each gene deletion in the pooled population were calculated by quantifying each barcode at different temperatures (**Fig. 1A, Table S1**). The relative fitness of the heat shock sample compared to the control at 30°C was used to identify genes whose deletion results in a change in fitness during heat shock (**Fig. 1A-B, Table S1**).

We observed that *B. subtilis* strains lacking the genes coding for the heat shock transcriptional repressors HrcA or CtsR exhibit higher fitness at 50°C compared to 30°C (**Fig. S1A**), consistent with their known regulatory role. In contrast, deletion of the genes coding for the DnaK chaperone system, the protease ClpP, and the adaptor protein complex McsA-McsB show greater sensitivity to increased temperatures (**Fig. S1B**), demonstrating that our screening approach can identify genes with already known heat-shock phenotypes[21–23].

The control of transcription initiation by transcription factors has been well established[24]. However, the contribution of RNA stability in stress response is not well understood. Interestingly, six mutants lacking RNases or RNase-regulating genes exhibit differential fitness at 50°C compared to 30°C (**Fig. 1B)**. The deletion of RNase Mini-III (Δ*mrnC)* results in lower fitness at 30°C, whereas its fitness remains unaffected at 50°C. Deletions of RNase J2 (Δ*rnjB)*, the nano-RNase A (Δ*nrnA*), and the RNA pyrophosphohydrolase and (p)ppGpp hydrolase NahA (Δ*yvcI*) exhibit reduced fitness during increased temperatures (**Fig. 1B**).

One of the mutants with the lowest fitness score at 50°C is Δ*ymcA* (**Fig. 1B**). YmcA (RicA) interacts with YaaT (RicT) and YlbF (RicF) to form the Y-complex, which associates with the endonuclease RNase Y for maturation of polycistronic mRNA and riboswitches[25,26]. In addition, we also identified Δ*yaaT* in our screen (**Fig. 1B**). We could confirm the heat sensitivity of all three deletion mutants of the Y-complex genes in single-culture experiments during a severe heat shock at 54°C (**Fig. 1C**).

Identification of Y-complex-dependent cleavages at late exponential and transition phases

We evaluated the growth of all three strains lacking the Y-complex encoding genes. They exhibit a similar growth defect that begins at the end of the exponential phase and continues during transition phase until the stationary phase (**Fig. 2A**). Given that this complex associates

with the endonuclease RNase Y and regulates substrate selection[26], we investigated Y-complex-dependent cleavages in the late exponential and transition phase (**Fig. 2A**) using the ISCP (Identification of Specific Cleavage Positions) approach[27]. We compared the coverage of RNA 3' and 5' ends in the WT and Δ*ymcA* mutant, and the ends significantly reduced in the Δ*ymcA* were classified as putative Y-complex-dependent cleavages (**Table S2**). It is worth noting that deleting any member of the Y-complex results in a significant decrease in the processing of substrate RNA[26]. When a transcript is cleaved, it results in two products: one is quickly degraded by exonucleases, while the other is stabilized[27]. Consequently, it is not always possible to detect both 5' and 3' ends after cleavage.

We identified 221 and 258 Y-complex-dependent ends in late exponential and transition phases, with six also detected in a previous study at the mid-exponential phase[26] (**Table S3**). In the late exponential phase, 5' and 3' ends are almost equally distributed, yet more 5*'* ends are detected in the transition phase (**Fig. 2B**).

It is known that the Y-complex and RNase Y generate fragments with differential stability in the mid-exponential phase[26]. Here, we evaluated the stability of the resulting fragments in the late exponential and transition phases by calculating the ratio of coverage upstream and downstream of the cleavage site (**Table S2**). We observed a trend toward stabilizing downstream fragments. However, upstream fragments can also be stabilized to a lesser extent (**Fig. S2A**). The ISCP method differentiates processing sites with blunt ends (Unique, U-type) or when it was further processed by exonucleases[27] (Stepped, S-type). Most S-types were found at the 3' ends, suggesting further processing by exonucleases, while most U-types were detected at 5' ends (**Fig. 2C**). This is consistent with the trend to stabilise the downstream fragment (**Fig. S2A**).

The Y-complex could target a particular sequence motif, thereby helping to recognize specific substrates. However, a motif search using U-type ends resembles the simple motif described for RNase Y in *B. subtilis*[28], *S. aureus*[29], and *S. pyogenes*[27], being most likely a G upstream of the cleavage site (**Fig. S2B**). Given the simple sequence motif, we investigated whether cleavages occur randomly in longer or more abundant transcripts. Notably, approximately 81% of targeted transcripts are cleaved only once, about 16% twice, and very few are cleaved multiple times (**Fig. S2C)**. Neither the length nor the abundance of a transcript predicts whether it is cleaved, suggesting that other factors influence where cleavages occur (**Fig. S2D-E, Table S4**). Recent studies have shown that the cleavage efficiency is multifactorial, depending on the sequence and secondary structures surrounding the cleavage site[28,30].

As we observed that RNA processing could result in fragments with different stability (**Fig. S2A**), we wondered if this could be a consequence of secondary structures protecting them from exonucleases. We used U-type ends and compared transcripts with the same cleavage

134 motif but not cleaved as controls. For the 5' ends, a strong decrease in the minimum free
135 energy ~25 nt downstream of the cleavage site indicated a possible secondary structure, while
136 the upstream fragment remained similar to the control (**Fig. 2D**). The upstream fragment's
137 lower stability may be due to its lack of secondary structure, making it accessible to 3'-5'
138 exonucleases. For the 3' ends, the more stable upstream fragment could form a possible
139 secondary structure starting 10 nt upstream of the cleavage site (**Fig. 2D**). The generation of
140 mRNA fragments with different stability might have a regulatory role in gene expression.

141 **Y-complex-mediated transcript cleavages and mRNA maturation**

142 Most detected Y-complex-dependent ends are inside ORFs, mainly in polycistronic mRNAs
143 (**Fig. 2E-F**), confirming the role of the Y-complex in the maturation and stoichiometry regulation
144 of co-transcribed genes[26]. An example is the *cggR-gapA* transcript, where the Y-complex
145 mediates cleavage in the coding sequence of *cggR* near the stop codon[25,26]. Cleavage renders
146 the *cggR* fragment less stable compared to the *gapA* fragment (**Fig. S3A**), thereby uncoupling
147 the transcript levels of these co-transcribed genes. Interestingly, we observed other cleavages
148 generating similar uncoupling of transcripts, such as in the gene encoding the endonuclease
149 YloC (**Fig. S3B**, **Table S2)**. In addition, cleavages in genes transcribed as monocistronic
150 mRNAs, such as *guaB,* suggest that the Y-complex could initiate their degradation (**Fig. S3C**,
151 **Table S2**).

152 We observe Y complex-dependent processing in 5', 3', and internal UTRs (**Fig. 2F**). Cleavages
153 in 5' UTR suggest a possible regulatory role by decreasing the abundance of the mRNA
154 containing them, as already described for riboswitches[26,31], or by producing a shorter version
155 of a 5' UTR, which could affect gene expression. Processing of 3' and internal UTR could
156 influence mRNA stability and polycistronic mRNA maturation. We observed that some 3' UTR
157 cleavages are located upstream of the Rho-independent terminator, decreasing the stability of
158 the upstream fragment and leaving an apparent more stable downstream fragment that
159 includes its terminator structure, as observed for *trxB* (**Fig. S3D**). This phenomenon has been
160 observed in *E. coli*, where RNase E cleaves upstream of the Rho-independent terminator[32,33].

161 In polycistronic mRNA maturation, we observed that Y-complex processes internal UTRs,
162 decoupling the RNA levels of coding fragments (**Fig. S3E-F**). For example, the *bipA-ylaH*
163 transcript is cleaved 21 nt after the *bipA* stop codon, rendering the upstream fragment less
164 stable than the *ylaH* fragment (**Fig. S3E**). We also observed a cleavage between the *fusA* (EF-
165 G) and *tufA* (EF-Tu) genes, both coding for translation elongation factors (**Fig. S3F**).

166

167

168 **The Y-complex targets translation and metabolism-related genes in the late exponential**
169 **phase**

170 We wondered if the Y-complex primarily processes transcripts bearing genes with specific
171 functions required for switching the growth phase. Therefore, we conducted an
172 overrepresentation analysis and observed that the most significantly enriched categories
173 pertain to "Metabolism" and "Information processing" (**Fig. 2G, Fig. S4A, Table S5**). Overall,
174 the Y-complex is predominantly involved in the processing of operons encoding genes for
175 carbon metabolism (e.g., glycolysis and gluconeogenesis), nucleotide metabolism (e.g.,
176 pyrimidine and purine biosynthesis), and amino acid biosynthesis and utilization (**Fig. 2G**). This
177 allows adjusting the utilization and biosynthesis of nutrients when they become limited. In
178 addition, all transcripts containing rRNA and ~50% of transcripts carrying genes encoding
179 translation factors and r-proteins are processed by the Y-complex (**Fig. 2G**).

180 The reduced RNA processing in the *ymcA* deletion strain results in significant changes in the
181 transcriptome (**Fig. S4B, Table S6-7**). Consequently, transcripts of certain pathways related
182 to metabolism and translation, among others, show maturation events that depend on the Y-
183 complex and also demonstrate differential expression upon deletion of *ymcA* (**Fig. 2G**, **Fig.**
184 **S4B**). This may result from either a direct or indirect effect of decreased RNA maturation
185 events. Our results suggest that the Y-complex and RNase Y are important for transitioning to
186 the stationary phase by processing transcripts related to translation and metabolism, which
187 may impact their stability and/or gene expression.

188 **The Y-complex targets ribosomes for degradation**

189 Several Y complex-dependent cleavages were detected in the rRNA sequence during both
190 growth phases, most of them being in the 23S rRNA during the late exponential phase (**Fig.**
191 **3A**). We detected cleavages in specific helices in the 23S and 16S rRNA, mainly in loops of
192 hairpin structures (**Fig. S5A-B**). These helices are accessible and primarily located close to
193 the A-site and the interface between the two ribosomal subunits (**Fig. S6**), which could be
194 recognized by the Y-complex and the endonuclease RNase Y, initiating ribosome degradation.

195 We confirmed the observed rRNA degradation via northern blots of 23S or 16S rRNA (**Fig. 3B**,
196 **Fig. S7A**). Deletion of *ymcA* strongly reduces the presence of rRNA degradation intermediates
197 during the late exponential phase. As ribosomes are assembled co-transcriptionally[34], we
198 inhibited transcription by adding rifampicin to cultures at the late exponential phase. We
199 observed that stopping transcription does not affect rRNA degradation of the 23S and even
200 raises the levels of 16S degradation intermediates, indicating that mature ribosomes are
201 degraded (**Fig. 3B**, **Fig. S7A**).

202 Cleavages within mature rRNA can trigger ribosome disassembly and degradation, which,
203 during the transition phase, coincides with translation downregulation through reduced
204 synthesis and inhibition of ribosome activity. This suggests that the Y-complex may be involved
205 in reducing ribosome levels to accommodate the new, slower growth rate. Ribosome
206 degradation has also been observed in *E. coli,* where it is initiated by the functionally equivalent
207 endonuclease RNase E, resulting in a decrease in ribosome levels of up to 50%[35].

208 To understand this process, we measured ribosome content via quantitative mass
209 spectrometry (**Table S8**), using all r-proteins as a proxy. When *B. subtilis* shifts from
210 exponential to the transition phase, we observed a coordinated reduction in r-protein levels
211 (**Fig. 3C**), indicating a decrease in ribosome levels. This reduction is highly impaired in Δ*ymcA*
212 (**Fig. 3C**), where the levels of r-proteins do not decline to the same degree as in the WT, likely
213 due to the reduced degradation of ribosomes.

214 Accumulation of (p)ppGpp leads to inhibition of transcription of rRNA and r-proteins[19,36] upon
215 shortages of nutrients during the transition to the stationary phase. To test if the deletion of
216 *ymcA* is interfering with this transcriptional downregulation, we measured the promoter activity
217 of the rRNA promoters *rrnJ* and *rrnB* and r-protein promoters of *rplK*, *rplJ*, and *rpsJ*. All these
218 promoters show similar downregulation in the late exponential and transition phases in both
219 WT and Δ*ymcA* strains (**Fig. 3D-E**, **Fig. S7B-D**), confirming that their transcriptional control
220 remains unaffected and is not the cause of the increased ribosome amounts in the Δ*ymcA*
221 strain.

222 Notably, we observed that the increased levels of ribosomes in a Δ*ymcA* strain led to the
223 accumulation of hibernating 100S ribosomes during the transition phase (**Fig. 3F**). This 100S
224 is no longer observed after the deletion of the gene encoding the hibernation factor *hpf*, which
225 triggers their formation[37,38] (**Fig. S7E**). The presence of hibernating ribosomes at this time point
226 indicates that functional and over abundant ribosomes in the Δ*ymcA* strain are sequestered
227 away from the actively translating pool through hibernation.

228 **(p)ppGpp and the Y-complex play a crucial role in regulating the levels of ribosomes**

229 Since ribosome levels and translation are lowered by (p)ppGpp under nutrient limitation or
230 other stresses, we wondered if there is a genetic interaction between the two systems. Deleting
231 *ymcA* in a strain that cannot synthesize (p)ppGpp [(p)ppGpp^0] leads to an even stronger growth
232 defect during the transition phase (**Fig. 4A**). The (p)ppGpp^0 strain, like Δ*ymcA*, shows impaired
233 reduction of ribosome levels during the transition phase (**Fig. 4B**). The double mutant
234 (p)ppGpp^0 Δ*ymcA* shows almost no reduction in ribosome quantities during this growth phase
235 (**Fig. 4B-C**). The same is observed when the r-protein mass fraction is calculated at the
236 transition phase (**Fig. 4D**). These experiments suggest that the Y-complex and (p)ppGpp

237 control ribosome levels and translation independently during post-exponential growth. The
238 absence of regulation by both systems results in a severe growth defect.

239 **Increased ribosome levels lead to protein aggregation during heat shock**

240 Since we discovered the Δ*ymcA* strain in a competition experiment during heat shock, we
241 explored whether the Y-complex is involved in lowering ribosome levels upon proteotoxic
242 stress. We evaluated the degradation of 23S and 16S rRNA by the Y-complex before and after
243 heat shock (**Fig. 5A**, **Fig. S8A**). After 15 minutes at 50°C, degradation intermediates are
244 observed in the WT but not in Δ*ymcA*, confirming a role of the Y-complex in degrading
245 ribosomes during heat stress (**Fig. 5A**). Comparing r-protein mass fractions before and during
246 heat shock shows that both WT and Δ*ymcA* downregulate ribosome levels during the
247 experiment. Overall, there are increased levels of r-proteins in the Δ*ymcA* strain already before
248 the heat shock (**Fig. 5B**), which suggests a role of the Y-complex in maintaining ribosome
249 levels during normal growth. Notably, the levels and induction of known heat-shock-regulated
250 proteins is not affected in the *ymcA* deletion (**Fig. 5C, Table S9, Fig. S8B**). This suggests that
251 chaperone and protease induction during heat stress in the Δ*ymcA* strain is intact.

252 The downregulation of translation is crucial to limit the increased burden of misfolding and
253 aggregation-prone nascent polypeptide chains on the PQC system. In agreement, a (p)ppGpp^0
254 strain shows increased aggregate formation during heat shock[7]. We quantified the relative
255 amount of aggregated proteins before and after 15 minutes of severe heat shock at 54°C and
256 observed that the Δ*ymcA* strain contained significantly higher amounts of aggregated proteins
257 already prior to heat exposure (**Fig. 5D**). This is consistent with the observed increased
258 ribosome levels of the Δ*ymcA* strain already without heat shock (time point 0 in **Fig. 5B**). After
259 15 minutes of heat shock, Δ*ymcA* shows 20% more aggregated proteins than WT. The
260 (p)ppGpp^0 Δ*ymcA* mutant exhibits even higher protein aggregation than Δ*ymcA* or (p)ppGpp^0
261 strains alone, further supporting that (p)ppGpp and the Y-complex act independently on the
262 regulation of ribosome levels and translation (**Fig. S8C**). Mutants of the Y-complex are also
263 strongly affected by other proteotoxic stresses, such as osmotic and oxidative stress, but not
264 by ethanol (**Fig. S8D**), which further demonstrates the importance of controlling ribosome
265 levels under proteotoxic stress conditions.

266 In summary, we observed that the Y-complex controls ribosome levels by degrading rRNA and
267 processing r-protein transcripts. The absence of the Y-complex leads to an increase in the
268 amount of ribosomes, resulting in a higher load on the PQC by nascent polypeptide chains,
269 which in turn may increase sensitivity to protein folding stresses.

270

Discussion

Regulation of transcription initiation plays a crucial role in controlling stress response pathways. Gene expression can also be controlled post-transcriptionally, e.g., by modifying mRNA stability or translation efficiency. Due to the short half-life of mRNA, their levels can change rapidly through transcription initiation, which may lead to the assumption that RNases do not play a direct role in regulating gene expression during stress. However, we observed that the fitness of *B. subtilis* during heat shock is affected by the deletion of some non-essential RNases and the Y-complex, which regulates substrate selection of the quasi-essential endonuclease RNase Y (**Fig. 1B-C**). This suggests that controlling RNA maturation and stability can play an important role in stress response and gene expression.

Our results suggest that the Y-complex may regulate transcripts involved in a wide range of metabolic pathways, developmental processes, stress responses as well as translation (**Fig. 2G, Fig. S4A-B, Table S2, Table S6-7**). RNA processing by the Y-complex-guided RNase Y could potentially create new transcript isoforms[26] or modify regulatory elements such as UTRs[26,31] (**Fig. 2F**, **Fig. S3**), thereby tailoring gene expression to specific growth conditions. This could explain some pleiotropic phenotypes already observed in these mutants, such as reduced sporulation, competence, and defective biofilm formation[39–41]. More research is necessary to understand the exact role of the Y-complex in developmental pathways.

We also show that the Y-complex initiates ribosome degradation at the end of exponential growth by directing RNase Y to cleave 23S and 16S rRNA (**Fig. 3A-B**, **Fig. S7A**), thereby decreasing ribosome levels. Consistent with our findings, it has been previously suggested that RNase Y could degrade rRNA in aging spores[42]. In *E. coli*, ribosome degradation is also triggered during nutrient starvation. This process is initiated by the endonuclease RNase E, which is functionally equivalent to RNase Y but does not share sequence homology, exemplifying a case of convergent evolution[43].

Recent evidence indicates that YmcA and YlbF transfer YaaT to RNase Y, forming a stable, membrane-localized YaaT-RNase Y complex[44]. However, the deletion of any of the Y-complex members leads to a strong decrease in the processing of target mRNA[26], indicating that all of them are equally indispensable for RNA processing. Both YmcA and YlbF show a dynamic localization between the cell membrane and the cytosol[45]. It is possible that YmcA and YlbF also recognize substrates, including ribosomes, and direct them to the membrane for cleavage. This represents a sophisticated spatial regulation of RNA processing and ribosome decay, separating them from transcription and translation in the cell.

RNase Y in *B. subtilis* also interacts in the membrane with other RNases, helicases, and glycolytic enzymes to form a degradosome-like network (DLN), which participates in the decay

306 of RNA[46–48]. This membrane localization would also imply that once rRNA is cleaved by RNase
307 Y and the Y-complex, exonucleases such as RNase R, PNPase, and RNase J could complete
308 its degradation. AAA+ protease complexes could degrade the released ribosomal proteins. For
309 instance, in *E. coli*, r-proteins are degraded by the Lon protease during starvation[49].

310 Most of the cleavages we observed in rRNA were located in the 23S (**Fig. 3A**); however, the
311 Y-complex and RNase Y can also initiate 16S degradation in the late stationary phase and
312 during heat shock (**Fig. 3A**, **Fig. S7**, **Fig. S8**). Recently, it was observed that the
313 exoribonuclease RNase R alone can degrade 16S[50], suggesting that endonucleolytic
314 cleavages might not be strictly necessary for 16S degradation. It is worth noting that RNase R
315 is induced as part of the general stress response, which is activated in the stationary phase or
316 during heat shock[51], indicating a possible stress-specific degradation of 16S rRNA
317 independent of the Y-complex. These observations suggest the presence of different possible
318 pathways for ribosome degradation.

319 Interestingly, ribosomes have been observed to reach membranes during starvation conditions
320 in several organisms. For instance, in *E. coli*, the hibernation factors YqjD/ElaB/YgaM can bind
321 to 70S ribosomes near the peptide exit tunnel and tether them to the inner membrane[52]. In
322 eukaryotes, during starvation, the proteins NUFIP1 and ZHNIT3 bind ribosomes and act as
323 cargo receptors in the forming autophagosome for their degradation[53]. Recently, it has also
324 been shown that, during nutrient scarcity, cytoplasmic ribosomes can hibernate by binding to
325 the mitochondrial membrane in yeast[54].

326 The regulation of translation by the Y-complex is not limited to ribosome degradation. The Y-
327 complex additionally processes transcripts encoding r-proteins and other translation factors
328 (**Fig. 2G**), such as BipA, EF-Tu, and EF-G (**Fig. S3**), which might regulate their translation or
329 lead to their decay. Strikingly, the Y-complex is necessary to process some transcripts coding
330 for r-proteins at the mid-logarithmic phase[26], and the depletion of RNase Y in similar conditions
331 leads to an increased abundance of transcripts of r-proteins, such as *rplS, rpsO, rpmA, rpsD,*
332 *rpsB,* and *rplU*[55].

333 Translation control is an important component of certain stress response mechanisms. For
334 example, during nutrient starvation, downregulating translation allows the reallocation of
335 resources to biosynthetic pathways[56]. During proteotoxic stresses, it could relieve the
336 overwhelmed PQC system by reducing the synthesis of new proteins that could potentially
337 aggregate[57]. The stress transcription factor Spx and the alarmones (p)ppGpp regulate
338 ribosome levels in *B. subtilis*, and the lack of both impairs growth at 50°C [7]. The strong growth
339 defect of cells lacking both (p)ppGpp and the Y-complex suggests that the two systems are
340 important for transitioning from the exponential to the stationary phase. Missing their combined
341 regulation of translation leads to high ribosome levels and increased accumulation of protein

342 aggregates (**Fig. S8C**). In times of nutrient limitation, the collective function of (p)ppGpp and
343 the Y-complex in regulating ribosome levels by inhibiting their synthesis and initiating
344 degradation allows resource allocation to other biosynthetic pathways (**Fig. 6**).

345 In conclusion, ribosome degradation is crucial during nutrient scarcity. Different organisms
346 employ various strategies to achieve ribosome degradation. We demonstrate that the Y-
347 complex and RNase Y are responsible for this function in *B. subtilis*, likely applicable to many
348 other bacteria that lack RNase E. Further studies are required to fully describe how this process
349 operates. This includes, for example, how ribosomes reach the membrane, whether and how
350 the Y-complex is activated during the late exponential phase, and which proteases are involved
351 in r-protein degradation.

352

353 **Materials and methods**

354 Growth conditions

355 Unless stated the contrary, strains (**Table S10**) were streaked on LB plates (5 g/l yeast extract,
356 10 g/l tryptone agar, 10 g/l NaCl, 1.5% agar) containing the required antibiotics for selection (1
357 µg/ml erythromycin + 25 µg/ml lincomycin, 150 µg/ml spectinomycin or 10 µg/ml kanamycin)
358 and incubated overnight at 37°C. A single colony was inoculated in 3 ml of LB medium and
359 grown overnight at 37°C and 180 rpm, then used as the inoculum for subsequent experiments.

360 Strain construction

361 For constructing the strains Δ*ymcA::erm*^{R} and Δ*yaaT::erm*^{R}, the loci containing the resistance
362 cassette were PCR-amplified from the respective strains of the BKE library[20] and transformed
363 in *B. subtilis* WT. The deletions of Δ*rel::kan*^{R} and Δ*ylbF::erm*^{R} were constructed as described
364 in Ref.[20]. For promoter activity reporter strains, the *gfp*(mut2) gene was cloned downstream of
365 the promoters of interest, using the integrative plasmid pDR111 as a backbone.

366 For transformation, 600 µl of an overnight culture of the receptor strains were diluted in 5 ml
367 competence medium (17.5 g/l K_2HPO_4, 7.5 g/l KH_2PO_4, 2.5 g/l $(NH_4)_2SO_4$, 1.25 g/l tri-sodium
368 citrate x2 H_2O, 0.5% glucose, 7 mM $MgSO_4$, 0.1 mg/ml L-tryptophan, 0.02% casamino acids,
369 0.22 g/ml ammonium iron citrate) and grown at 37°C, 180 rpm, for 3 hours. Subsequently, 5
370 ml of starvation medium (17.5 g/l K_2HPO_4, 7.5 g/l KH_2PO_4, 2.5 g/l $(NH_4)_2SO_4$, 1.25 g/l tri-sodium
371 citrate x2 H_2O, 0.5% glucose, 7 mM $MgSO_4$) were added and grown for 2 more hours. One ml
372 of this culture was incubated with the DNA to be transformed and grown for 2 hours at 37°C
373 and 180 rpm. Positive clones were selected on LB agar containing the required antibiotics.
374 Genetic modifications were verified using PCR and DNA sequencing.

375 Genetic screening during heat shock

376 The BKE library[20] was replicated on LB agar plates containing 1 µg/ml erythromycin. Liquid
377 cultures were prepared in 200 µl LB medium supplemented with 1 µg/ml erythromycin and
378 grown for 42 hours at 30°C 200 rpm. All mutant strains were pooled and mixed for 15 minutes
379 using a magnetic stirrer. The pooled culture was centrifuged at 5000 rpm for 10 minutes at
380 18°C. The pellet was resuspended in LB medium to an OD_{600} of 65 and mixed with an equal
381 volume of 50% glycerol. The pooled library was aliquoted and kept at -80°C.

382 For each replicate, a tube of the pooled library was quickly unfrozen in a water bath at 30°C
383 and used to inoculate 75 ml LB medium in 500 ml flasks to a starting of OD_{600} 0.05. The culture
384 was grown in a water bath at 30°C, 180 rpm, until OD_{600} 0.4. Fifty ml of culture were split into
385 two 250 ml flasks. One flask was transferred to 50°C, 180 rpm for heat shock. The other flask
386 was used as a control sample and was kept at 30°C. One ml samples were collected for gDNA

387 purification at 0 and 2 hours post temperature shift. Samples were pelleted for 2 minutes at
388 13,000 rpm and washed once with 500 µl PBS. gDNA was purified using the Wizard® Genomic
389 DNA Purification Kit (Promega, A1120) and stored at -20°C until further processing.

390 The strain-specific barcodes were amplified using indexed primers (**Table S7**) with the Collibri
391 Library Amplification Master Mix (ThermoFisher, A38539050) according to the manufacturer's
392 instructions, with 100 ng of gDNA as input, for 22 cycles. Barcodes were gel-purified,
393 quantified, pooled equimolarly, and sequenced using the Illumina NovaSeq2 single-read
394 method at the Sequencing Core Facility of the Max Planck Institute for Molecular Genetics
395 (Berlin, Germany).

396 To calculate the fitness score of each deletion mutant from barcode abundance, BEAN-counter
397 v2.6.1 was used with the following settings. A fixed amplicon read structure was used with an
398 index at position 0, the common primer sequence GCAGGCGAGAAAGGAGAG at position 9,
399 and the mutant barcode at position 27 of read 1. All other settings were used with default
400 values. The sample before heat shock served as a reference to which all other time points
401 were compared. All comparisons were performed with three biological replicates.

402 Fitness data was further analyzed using the R statistical computing language (v4.3.3). For
403 annotation, protein-related information was fetched using the Uniprot REST API (29 February
404 2024). Average fitness per gene, condition, and time point was calculated as the arithmetic
405 mean of the fitness score from three biological replicates. Differential fitness ΔF, e.g. for
406 comparison of treatment *versus* control at a particular time point, was calculated as $\Delta F =$
407 $F_{treatment} - F_{control}$. A two-sided Student's t-test was performed to evaluate statistical significance
408 for each gene, and the obtained *p*-value was corrected using the Benjamini-Hochberg
409 procedure[58].

410 Growth curves

411 Twenty-five ml of LB medium were inoculated with an overnight culture to a starting OD_{600} 0.05
412 in 250 ml Erlenmeyer flasks. Cultures were grown at 37°C 180 rpm in a water bath. OD_{600} was
413 monitored every 30 minutes. The average and standard deviation of three biological replicates
414 were calculated.

415 Heat shock survival

416 Cultures were inoculated in 25 ml LB medium to OD_{600} 0.05 and incubated in a water bath at
417 37°C 180 rpm. At OD_{600} 0.3 – 0.4, the cultures were exposed to a heat shock at 54°C for 2
418 hours, and samples for viability measurement were obtained every 30 minutes. Viability was
419 measured by spotting 4 µl of 1:10 serial dilutions in PBS of each sample on LB agar. The plates
420 were incubated overnight at 30°C, and the colony-forming units (CFU) were counted. The

421 CFU/ml was calculated for each sample, and relative viability was determined using samples
422 before heat shock as a reference.

423 Isolation of protein aggregates

424 Twenty-five ml of culture were harvested before and 15 minutes after heat shock at 54°C by
425 centrifugation for 5 minutes at 10,000 rpm. The pellets were washed once with buffer A (100
426 mM HEPES pH 8.0, 150 mM NaCl) and lysed by bead-beating in buffer B (100 mM HEPES
427 pH 8.0, 150 mM NaCl, cOmplete EDTA-free protease inhibitor) using 0.1 mm glass beads.
428 Afterwards, samples were centrifuged at 1000 x *g* for 2 minutes to obtain the cell extract. The
429 soluble fraction was separated from protein aggregates by centrifugation for 15 minutes at
430 11,000 x *g* at 4°C. To remove membrane proteins, the aggregates were resuspended in buffer
431 B containing 1% Triton X-100 and incubated for 1 hour at 4°C. Protein aggregates were
432 recovered by centrifugation at 11,000 x *g*, 4°C for 15 minutes and resuspended and incubated
433 as described above. Protein aggregates were washed again with buffer B + 0.5% Triton X-
434 100, and the detergent was removed in a final wash using buffer B. Pellets containing protein
435 aggregates were resuspended in buffer B + 2% SDS by boiling for 5 minutes at 95°C. Protein
436 concentration was measured using the Rapid Gold BCA Protein-Assay-Kit (Pierce™, A53225).
437 The percentage of aggregated protein was calculated to the total protein content in the cell
438 extract.

439 Spot test

440 Overnight cultures were diluted 1:1000 in LB medium without antibiotics and incubated at 37°C
441 180 rpm for 7-8 hours. The cultures were diluted to OD_{600} 1 in fresh LB medium in a 96-well
442 plate. Seven serial 1:10 dilutions were prepared in 1x PBS. Four µl of each dilution was spotted
443 on LB agar containing different stressors (concentration indicated in the figures). Plates were
444 freshly prepared before use.

445 RNA purification

446 Samples for RNA purification were collected at the indicated time points: exponential phase
447 (OD_{600} ~ 0.3), late exponential phase (OD_{600} ~ 1) and transition phase (100 minutes after late
448 exponential phase). Rifampicin was added to a final concentration of 100 µg/ml for 10 minutes.

449 Samples were harvested by mixing with the same volume of cold 1:1 acetone:ethanol and
450 centrifugated at 9,000 rpm for 5 minutes, 4°C. RNA purification was performed according to
451 Ref.[27] with slight modifications: The pellet was washed twice in 1 ml TE-sucrose buffer (50 mM
452 Tris-HCl pH 8.0, 10 mM EDTA, 25% sucrose) and centrifugated at 10,000 rpm for 5 minutes,
453 4°C. Cells were resuspended in 130 µl lysis buffer (20 mM Tris-HCl pH 8.0, 50 mM EDTA, 20
454 % sucrose) supplemented with 3.2 mg/ml lysozyme and incubated on ice for 5 minutes. Two
455 hundred µl of lysis executioner (2% SDS, 1 mg/ml Proteinase K) were added to the samples

456 and incubated at 95°C for 1.5 minutes. Samples were mixed with 1 ml of TRIzol (Ambion) and
457 incubated at room temperature. After 5 minutes, 250 µl chloroform was added to each sample
458 and mixed by vortexing. After 10 minutes at room temperature, the samples were centrifuged
459 for 10 minutes at 11,000 rpm. The RNA was isopropanol-precipitated at -20°C overnight. RNA
460 was pelleted at 11,000 rpm for 20 minutes at 4°C, washed with 1 ml 70% ethanol followed by
461 another centrifugation at 13,000 rpm for 10 minutes at 4°C. The pellet was air-dried and
462 resuspended in 50 µl nuclease-free water.

463 ISCP RNA sequencing

464 RNA sequencing was performed as previously described[59]. In brief, total RNA was treated with
465 TURBO DNase (Ambion, AM2238), depleted of ribosomal RNA using the riboPOOL rRNA
466 depletion kit for *B. subtilis* (siTOOLS; two reactions with 4.5 µg each) and purified using the
467 RNA Clean & Concentrator-5 kit (RCC-5; Zymo Research). RNA 5' triphosphates were
468 converted to monophosphates using RppH (NEB), and RNA was recovered using
469 phenol:chloroform:isoamyl alcohol extraction followed by ethanol precipitation. RNA ends were
470 repaired using T4 Polynucleotide Kinase (Thermo Scientific), before RNA was purified using
471 the RCC-5 kit and fragmented using an M220 Focused-ultrasonicator (Covaris) as described
472 by the manufacturer but with a treatment time of 100 s (microTUBE AFA Fiber Snap-Cap). After
473 purification using the RCC-5 kit, sequencing libraries were prepared from the recovered RNA
474 using the NEXTflex Small RNA-Seq Kit v3 (Bioo Scientific) according to the manufacturer's
475 protocol (including step G). Libraries were purified as described in step I of the NEXTflex Rapid
476 Directional qRNA-Seq Kit (Bioo Scientific) using Agencourt AMPure XP Beads (Beckman
477 Coulter; 0.9x bead-to-sample ratio). Sequencing was performed on an Illumina NovaSeq 6000
478 in paired-end mode with a read length of 100 bp at the Sequencing Core Facility of the Max
479 Planck Institute for Molecular Genetics (Berlin, Germany).

480 Processing of RNA sequencing data

481 FastQC (v0.11.5) was used to assess the quality of the data. Reads were filtered with a
482 minimum quality score of 10 and a length of at least 18 nt, cleaned from adapter sequences
483 using Cutadapt (v3.5)[60], and mapped against the *B. subtilis* reference genome (NC_000964.3)
484 using STAR (v2.7.10a_alpha_220314)[61] in 'random best' and 'end to end' modes. Resulting
485 BAM files were sorted and indexed with Samtools (v1.9)[62], and PCR duplication artefacts were
486 removed using UMI Tools (v1.1.0)[63]. Gene counts of annotated RefSeq genes were
487 determined with featureCounts (v2.0.3)[64] and differentially expressed genes (DEG) were
488 calculated with three replicates per condition and time point using DESeq2 (v1.24.0)[65]. *p*-
489 values were corrected for multiple testing using the Benjamini-Hochberg method[58]. To call
490 DEGs, a threshold of adjusted *p*-value < 0.05 and absolute log2 fold change > 1 was used.

491 Genome coverage profiles (total, 5' and 3' ends) were generated using a custom script utilizing
492 the HTSeq library (v2.0.2)[66]. We performed the aforementioned analysis steps using a
493 customized pipeline implemented in Snakemake (v7.14.0)[67].

494 Identification of Y complex cleavage sites

495 The Y-complex-dependent cleavage positions were identified following the previously
496 published procedure[59]. In brief, the genome coverage data was prefiltered with a count per
497 million (cpm) value ≥0.05, and only the RNA ends displaying a cpm ≥ 5 were further analyzed.
498 We carried out differential expression analysis of normalized 5′ and 3′ read ends by comparing
499 WT vs. Δ*ymcA* at the late exponential and transition phase. Y-complex-dependent ends were
500 identified using edgeR (v3.28.0)[68] with absolute log2 fold change ≥ 1 and FDR < 0.05, and kept
501 only if present in both comparisons. These results were further filtered with additional
502 parameters, i.e., the "proportion of ends (cleavage ratio)" and the "ratio of WT and Δ*ymcA*
503 proportion of ends" as was previously described[59]. Moreover, to reduce the potential set of
504 false positive processing sites even further, we applied an additional cut-off on the "proportion
505 of ends" parameter, i.e., we kept only processing sites with a cleavage ratio of the reference
506 strain (WT) ≥ 95%-percentile of the cleavage ratio of the mutant strain.

507 Impact of processing sites on transcript and operon expression

508 To examine the impact of cleavage sites on transcript and operon expression, as well as other
509 genomic features such as untranslated regions (UTRs) and regulatory elements, we calculated
510 transcript per million (TPM) values from variance-stabilized data for each annotated RefSeq
511 gene (transcript level) and for each operon as defined in the BSGatlas (v1.1)[69] using the
512 DESeq2 package and a custom Python script. Furthermore, all Y-complex-dependent
513 cleavage sites were mapped to various genomic features, including coding regions, UTRs,
514 terminator regions, and riboswitches, as defined in the BSGatlas[69] (**Table S2**).

515 Processing site sequence logo

516 The sequence logos were generated with Logomaker (v0.8)[70], specifically for 5' and 3' end U-
517 type cleavage sites. For this, we extracted 30 nt sequences centered at the cleavage site and
518 calculated the logos with a GC content of 43.5%.

519 RNA secondary structure prediction

520 The RNA structure surrounding Y-complex-dependent cleavage sites was estimated by
521 calculating the MFE (ΔG in kcal/mol) utilizing RNAfold (v2.6.4)[71]. This analysis employed a
522 sliding window approach with 50 nt sequences, focusing on a 200 nt region centered around
523 the position of interest. The average MFE at each nucleotide was then calculated. To calculate
524 and visualize the background folding energy, we randomly draw potential processing sites from

525 the genome determined with the corresponding 5' or 3' end motif and calculate the average
526 MFE at each nucleotide as described above. Potential processing sites were drawn 50 times
527 independently.

528 Overrepresentation analysis

529 Annotations of operons were obtained from BSGatlas[69] and gene categories from Subtiwiki
530 (24 July 2023)[72]. The overrepresentation analysis was performed using the R statistical
531 computing language (v.4.2.2) and the Bioconductor package Category (v.2.64.0).

532 Northern blot

533 Biotinylated RNA probes were prepared using the HighYield T7 Biotin11 RNA Labeling Kit
534 (UTP-based) (Jena Bioscience, RNT-101-BIOX) from PCR amplified fragments containing the
535 promoter for the T7 RNA polymerase (**Table S11**). Probes were purified using the Monarch®
536 Spin RNA Cleanup Kit (NEB, T2040) according to the manufacturer's instructions. Probes were
537 designed taking into consideration the predicted cleavage sites.

538 One and a half µg of total RNA was separated on denaturing agarose gels (1% agarose,
539 20 mM MOPS, 5 mM NaOAc, 1 mM EDTA, 6.6% formaldehyde, pH 7.0) in 1x AGE-NB
540 Running Buffer (20 mM MOPS, 5 mM NaOAc, 1 mM EDTA, 0.74% formaldehyde, pH 7.0).
541 The gel was washed 3 times with milli-Q water and once with 10x SSC buffer, and the
542 nitrocellulose membrane was washed once with milli-Q water and once with 10x SSC. The
543 RNA was transferred using a vacuum blotter at 300 mbar covered with 10x SSC for 1.5 hours.
544 After transfer, the membrane was washed for 2 minutes with 6x SSC, once with water, and
545 dried and crosslinked at 254 nm 0.12 J twice. The membrane was developed with methylene
546 blue, and the staining was removed by washing with 0.2x SSC containing 1% SDS, followed
547 by washing with milli-Q water. The hybridization of 16S or 23S rRNA probes was performed
548 using the North2South Chemiluminescent Hybridization and Detection Kit (Thermo) and
549 North2South Hybridization Stringency Wash Buffer (2X) according to the manufacturer's
550 instructions. Blots were developed in a Vilber imaging system.

551 RT-qPCR

552 Twenty µg of total RNA were treated with TURBO DNase (Ambion, AM2238) and purified using
553 the Monarch® Spin RNA Cleanup Kit (NEB, T2040). Subsequently, cDNA was prepared using
554 the LunaScript RT Mastermix (NEB, E3025) and 2.5 µg of DNase-treated RNA as input.
555 Quantitative PCR was performed using the Luna Universal qPCR Master Mix (NEB, M3003)
556 in a QuantStudio 5 Real-Time PCR System (Applied Biosystems). To calculate changes in *gfp*
557 transcription, samples from the late exponential and transition phases were compared to those

558 from the exponential phase, with *pcp* serving as a reference gene using the Pfaffl method[73].
559 Primers used for RT-qPCR are listed in **Table S11**.

560 Ribosome sedimentation in sucrose gradients

561 Cultures of WT and Δ*ymcA* were grown until the exponential phase (OD_{600} ~ 0.3), late
562 exponential (OD_{600} ~ 1), and transition phase (100 minutes after the late exponential phase).
563 Chloramphenicol was added at a concentration of 100 µg/ml 2 minutes prior to sample
564 collection. Fifty ml of culture were pelleted at 4,500 rpm for 10 minutes at room temperature.
565 Pellets were transferred to ice and resuspended in 2 ml of lysis buffer (20 mM Tris-HCl pH 8.0,
566 100 mM NH_4Cl, 10 mM $MgCl_2$, 0.4% Triton X-100, 0.4% NP-40, 1 mM chloramphenicol, 100
567 U/µl DNase I), and flash-frozen. Cells were lysed under cryogenic conditions using 5 cycles of
568 mix-milling at 30 Hz for 1 minute. Lysates (240 µg RNA) were laid over a 10-50% sucrose
569 gradient in 20 mM Tris-HCl pH 8.0, 100 mM NH_4Cl, 10 mM $MgCl_2$, 0.5 mM DTT and resolved
570 at 35,000 rpm for 3 hours at 4°C. Gradients were analyzed using a piston fractionator (Biocomp
571 instruments), and absorbance at 260 and 280 nm was monitored.

572 Sample preparation for MS-based proteomics

573 Samples were collected at the indicated time points: late exponential phase (OD_{600} ~ 1) and
574 transition phase (100 minutes after the late exponential phase). For the proteomic changes
575 during heat shock, cultures were grown at 37°C until OD_{600} ~ 0.3 and shifted to 54°C. Samples
576 were collected at 0, 15, 30, and 60 minutes after heat shock. Ten ml of culture were collected
577 by centrifugation at 4,500 rpm for 10 minutes, and the pellet was stored at -80°C until further
578 processing.

579 Cell pellets were resuspended in 1 ml of cold PBS and centrifuged at 13,000 rpm for 5 minutes
580 at 4°C. The pellet was washed once more with PBS, resuspended in 150 µL of lysis buffer
581 (100 mM HEPES pH 8.0, 2% SDS, 20 mM TCEP, 60 mM CAA), and lysed using bead beating.
582 Cell debris was discarded by centrifuging at 13,000 rpm for 5 minutes at 4°C. The supernatant
583 was boiled at 95°C for 5 minutes, cooled down to room temperature, and the protein
584 concentration was estimated using the Rapid Gold BCA protein assay kit (Pierce). Samples
585 were flash-frozen in liquid nitrogen and stored at -80°C until further processing.

586 All samples were subjected to SP3 sample preparation[74] on an Agilent BRAVO liquid handling
587 robot. Ten µg of a 1:1 mixture of hydrophilic and hydrophobic carboxyl-coated paramagnetic
588 beads (SeraMag, #24152105050250 and #44152105050250, GE Healtcare) were added for
589 each µg of protein. Protein binding was induced by the addition of acetonitrile to a final
590 concentration of 50% (v/v). Samples were incubated at room temperature for 10 minutes. The
591 tubes were placed on a magnetic rack, and beads were allowed to settle for 3 minutes. The
592 supernatant was discarded, and beads were rinsed three times with 200 µL of 80% ethanol

593 without removing the tubes from the rack. Beads were resuspended in digestion buffer
594 containing 50 mM triethylammonium bicarbonate and both Trypsin (Serva) and Lys-C (Wako)
595 in a 1:50 enzyme-to-protein ratio. Protein digestion was performed for 14 hours at 37°C in a
596 PCR cycler. Afterward, the supernatant was recovered and dried down in a vacuum
597 concentrator.

598 Proteomics using Mass spectrometry

599 All samples obtained during the late exponential and transition phase were analyzed on an
600 Orbitrap Exploris (Thermo Scientific) equipped with a FAIMS Pro device and coupled to a 3000
601 RSLC nano UPLC (Thermo Scientific). Samples were loaded on a PepMap trap cartridge (300
602 µm i.d. x 5 mm, C18, Thermo) with 2% acetonitrile and 0.1% TFA at a flow rate of 20 µl/min.
603 Peptides were separated over a 50 cm analytical column (Picofrit, 360 µm O.D., 75 µm I.D.,
604 10 µm tip opening, non-coated, New Objective) that was packed in-house with Poroshell 120
605 EC-C18, 2.7 µm (Agilent). Solvent A consists of 0.1% formic acid in water. Elution was carried
606 out at a constant flow rate of 300 nl/min using a 60-minute method: 8-30% solvent B (0.1%
607 formic acid in 80% acetonitrile) within 23 minutes, 30-45% solvent B within 3 minutes, 45-98%
608 buffer B within 0.5 minutes, followed by column washing and equilibration. Data acquisition on
609 the Orbitrap Exploris was carried out using a data-dependent acquisition (**DDA**) method in
610 positive ion mode. MS survey scans were acquired from 375-1500 m/z in profile mode at a
611 resolution of 60,000. AGC target was set to 200% at a maximum injection time of 25 ms.
612 Peptides with charge states 2-6 were isolated within a window of 1.2 m/z and subjected to
613 HCD fragmentation at a normalized collision energy of 27%. The MS2 AGC target was set to
614 200%, allowing a maximum injection time of 22 ms. Product ions were detected in the Orbitrap
615 at a resolution of 15,000. Precursors were dynamically excluded for 20 s. The cycle time was
616 set to 1 s for each of the two FAIMS voltages of −45 and −65 V.

617 LC-MS/MS analysis of the heat shock samples was performed on an Ultimate 3000 UPLC
618 coupled to a Lumos hybrid mass spectrometer (Thermo Scientific). Peptides were loaded onto
619 a PepMap trap cartridge (300 µm i.d. x 5 mm, C18, Thermo) with 2% acetonitrile and 0.1%
620 TFA at a 20 µl/min flow rate. Peptides were separated over a 50 cm analytical column (Picofrit,
621 360 µm O.D., 75 µm I.D., 10 µm tip opening, non-coated, New Objective) that was packed in-
622 house with Poroshell 120 EC-C18, 2.7 µm (Agilent). Solvent A consists of 0.1% formic acid in
623 water. Elution was carried out at a constant flow rate of 250 nl/min using a 60-minute method:
624 8-30% solvent B (0.1% formic acid in 80% acetonitrile) within 23 minutes, 30-45% solvent B
625 within 3 minutes, 45-98% buffer B within 0.5 minutes, followed by column washing and
626 equilibration.

627 The mass spectrometer was operated in data-independent acquisition (**DIA**) and positive
628 ionization mode. MS1 full scans (375–1500 m/z) were acquired with a resolution of 60,000, a

normalized automatic gain control target value of 120%, and a maximum injection time set to 55 ms. Peptide fragmentation was performed using higher energy collision-induced dissociation and a normalized collision energy of 30%. MS2 spectra were acquired with a resolution of 30,000 (first mass 100 m/z) with 8 m/z DIA windows between 400 and 1200 m/z. A normalized automatic gain control target value of 100%, and a maximum injection time of 54 ms.

Proteomics data analysis

For samples at the late exponential and transition phase, Raw files were processed with MSFragger v3.5 using the default settings. Briefly, peak lists were extracted from raw files and searched using a Uniprot *Bacillus subtilis* database (v220530, taxonomy ID 224308) and a database containing sequences of common contaminants and decoys. Trypsin/P was set as enzyme specificity, allowing a maximum of two missed cleavages. Peptide matches were filtered to 1% FDR using PeptideProphet and Philosopher (v4.4.0).

For samples during heat shock, DIA-NN (DIA-NN v1.8.1) was employed for DIA data analysis. The main DIA-NN report, “report.txt”, was used for all calculations. Fasta file (Bacillus_subtilis_Strain168_UP000001570.fasta) was digested with a maximum of one missed cleavage. Peptide length was restricted from 7 to 30 peptides, and the precursor m/z range was set from 300 to 1800. N-terminal methionine excision was enabled. Cysteine carbamidomethylation was selected as a fixed modification, and methionine oxidation and N-terminal acetylation as variable modifications. The maximum number of variable modifications was set to two. All other parameters were at default settings, including the 1% precursor FDR and enabled match between runs (MBR). The main DIA-NN report, “report.pg_matrix.tsv,” was used for all calculations.

The R statistical computing language was used for data processing (v4.4.1). The main comparison of WT, Δ*ymcA*, (p)ppGpp^{0,} and (p)ppGpp^{0} Δ*ymcA* mutants was based on samples from data-dependent acquisition (DDA) experiments. Raw peptide intensity values from label-free quantitation were imported as tabular output from MSFragger. The MSstats package (v4.12.1)[75] was used to convert raw intensities to an MSstats experiment. In this process, peptide quantification data was $\log_2$-transformed, median-normalized, and summarized to protein abundance. All features mapping to a protein were used for quantification, Tukey’s median polish was used as a summarization strategy, and missing values were imputed using MSstats’ default strategy. Feature abundance and inferred protein quantity were visually inspected using profile plots. Experimental groups were compared using MSstats’ *groupComparison* function, and the similarity of conditions and replicates was inspected using principal component analysis (PCA, function *prcomp*). For annotation, protein-related information was fetched from Uniprot using the Uniprot REST API (14 June 2024). In addition

665 to the DDA experiments, a time series of WT and Δ*ymcA* mutants was obtained using data-
666 independent acquisition (DIA) proteomics. To quantify relative changes, the $\log_2$ fold change
667 of each time point was calculated using the zero time point as a reference. To quantify absolute
668 protein abundance for the ribosomal proteome sector, the coarse-graining strategy was used
669 as in Ref.[76,77]. Briefly, two protein sectors (groups) were created containing all annotated
670 proteins of ribosomal subunits. Raw MS1 intensities for all proteins of the respective group and
671 time points were summed up and divided by the total sum of protein intensities, yielding the
672 protein mass fraction per sector.

673 **Data availability**

674 Amplicon-seq and RNA-seq raw reads have been deposited at the European Nucleotide
675 Archive (ENA) under accession number PRJEB90661. Raw proteomic data have been
676 deposited at the PRIDE database under the accession number PXD065465 for DDA
677 proteomics of late exponential and transition phase samples. The DIA proteomics raw data
678 from the heat shock experiment can be accessed using the accession number PXD065462.

679 **Author contributions**

680 K.T., K.D., and F.A.C.; Conceptualization. K.D., F.A.C., K.T., R.A.-B., T.F.W., and K.A.:
681 Methodology. F.A.C., K.D., K.S., V.S., K.H., and F.K.: Investigation. K.D., F.A.C., R.A.-B., M.J.,
682 K.A., S.R., and K.T.: Formal analysis. F.A.C., K.D., R.A.-B., M.J.: Visualization. F.A.C., K.D.,
683 and K.T.: Writing – Original Draft. K.T. and E.C.: Funding acquisition. All authors: Writing –
684 Review & Editing.

685 **Acknowledgments**

686 This work was funded by the Deutsche Forschungsgemeinschaft (Tu106/8, SPP1879 for K.D.
687 and K.T., Leibniz Prize for E.C.) and the Max Planck Society (for E.C. and K.T.).

688

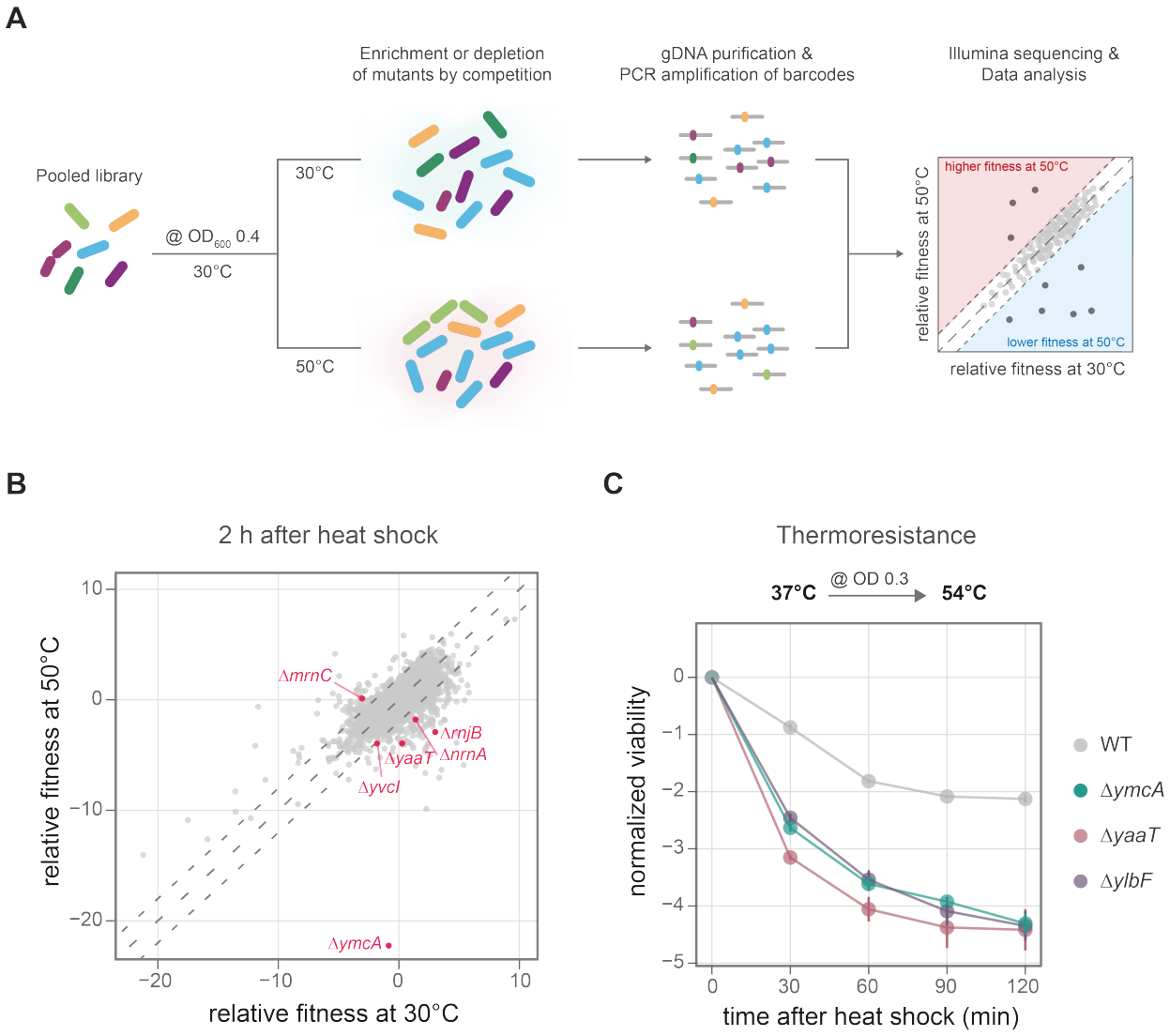

Figure 1. Genetic screening for genes involved in the heat shock response. A) Genetic screening experiment: the pooled library of deletion mutants (BKE) was grown at 30°C; when it reached an OD_{600nm} of 0.4, one fraction was exposed to 50°C while the other was maintained at 30°C. Genomic DNA (gDNA) was extracted from the library, and barcodes were amplified and sequenced using Next-Generation Sequencing. The fitness of each mutant at the mentioned temperatures and time points was calculated using BEANcounter. **B**) Relative fitness of each deletion mutant at 50°C (*y*-axis) and 30°C (*x*-axis) two hours post-temperature shift. Each point represents a deletion mutant, with mutants lacking RNase-related genes highlighted in magenta. The dotted lines indicate the range in which the relative fitness between the conditions differed by less than 2. Data represent the average of three biological replicates. A negative relative fitness value means that the abundance of the deletion mutant, compared to the rest of the population, was negatively affected by the treatment, while a positive value means an increased abundance in this condition. **C)** Changes in the viability (log_{10}CFU/ml) of WT and *ymcA, ylbF,* and *yaaT* deletion mutants to a severe heat shock at 54°C. Values were normalized to the viability at timepoint 0 min. The data represents the average ± standard error of three biological replicates.

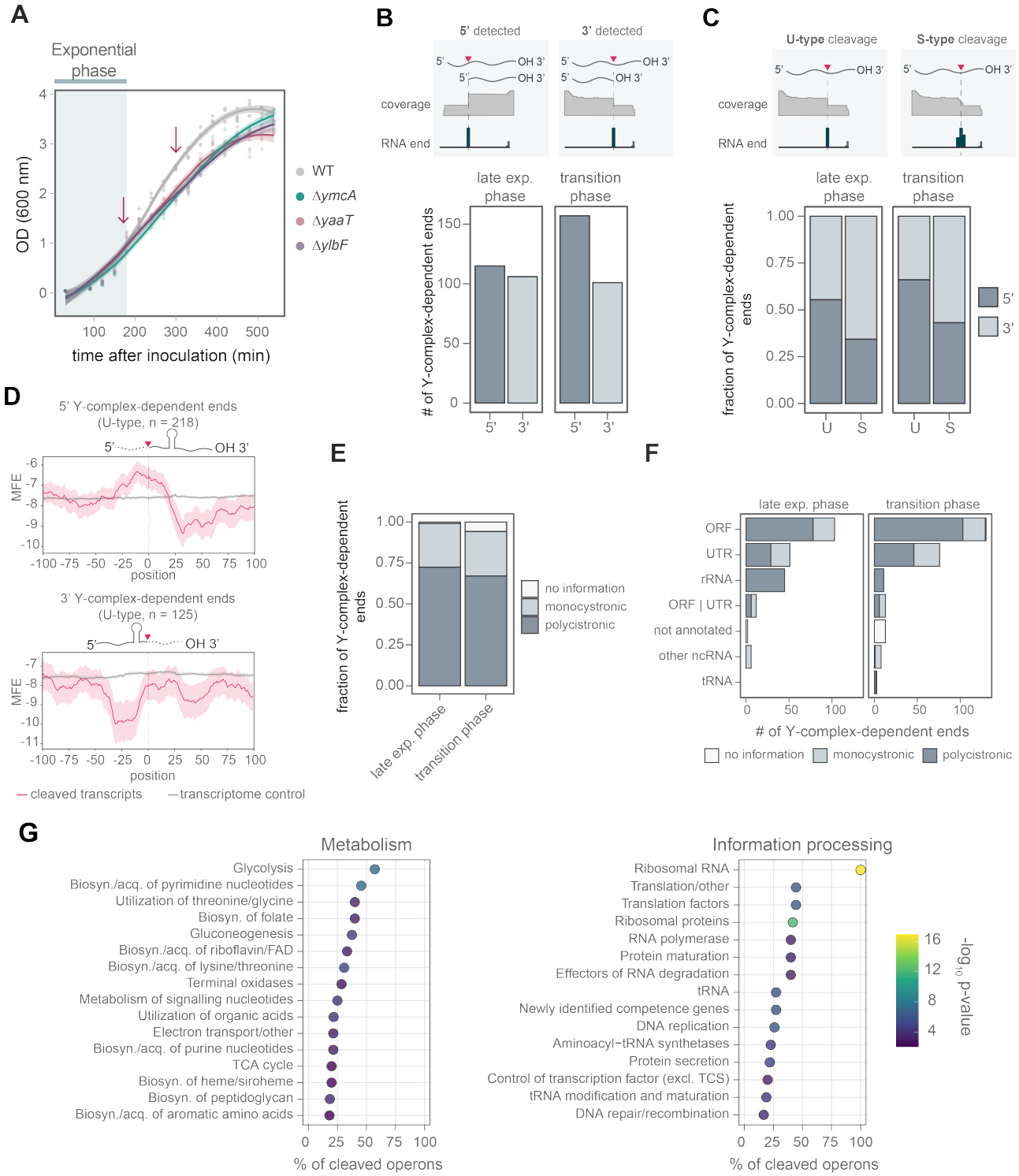

Figure 2. Identification of Y-complex-dependent cleavages at late exponential and transition phase. A) Growth curves of WT, *ymcA*, *ylbF*, and *yaaT* deletion mutants in LB at 37°C. The blue bar marks the exponential phase. Arrows indicate sample collection for the ISCP method at the late exponential and transition phases. Three biological replicates are displayed with a smooth curve regression. **B)** Number of RNA 3' or 5' ends identified at the two growth phases. **C)** Fraction of identified 3' or 5' ends displaying U-type (unique) or S-type (stepped) profiles. **D)** Minimum free energy (MFE) was calculated on 50 nt windows for RNAs cleaved by the Y-complex with U-type ends (in magenta). Transcripts that share the same cleavage motif but are not processed were used as a control (in gray). rRNA genes were excluded from the analysis since they are highly structured. **E)** Fractions of ends identified in genes transcribed in polycistronic or monocistronic RNA. **F)** Count of RNA features where

716 Y-complex-dependent ends are detected at either growth phase. Annotations were obtained from
717 BSGatlas[69]. **G)** Overrepresentation analysis of pathways whose transcripts are cleaved by the Y-
718 complex during the late exponential phase. Operons were assigned to be involved in a pathway if they
719 code for one gene participating in such a pathway. As genes in the same operon can have different
720 functions, transcripts may be linked to multiple roles. Pathway annotations were retrieved from
721 SubtiWiki[72]. The color indicates the statistical significance of the enrichment. Biosyn = biosynthesis, acq
722 = acquisition, excl TCS = excluding two-component systems.

723

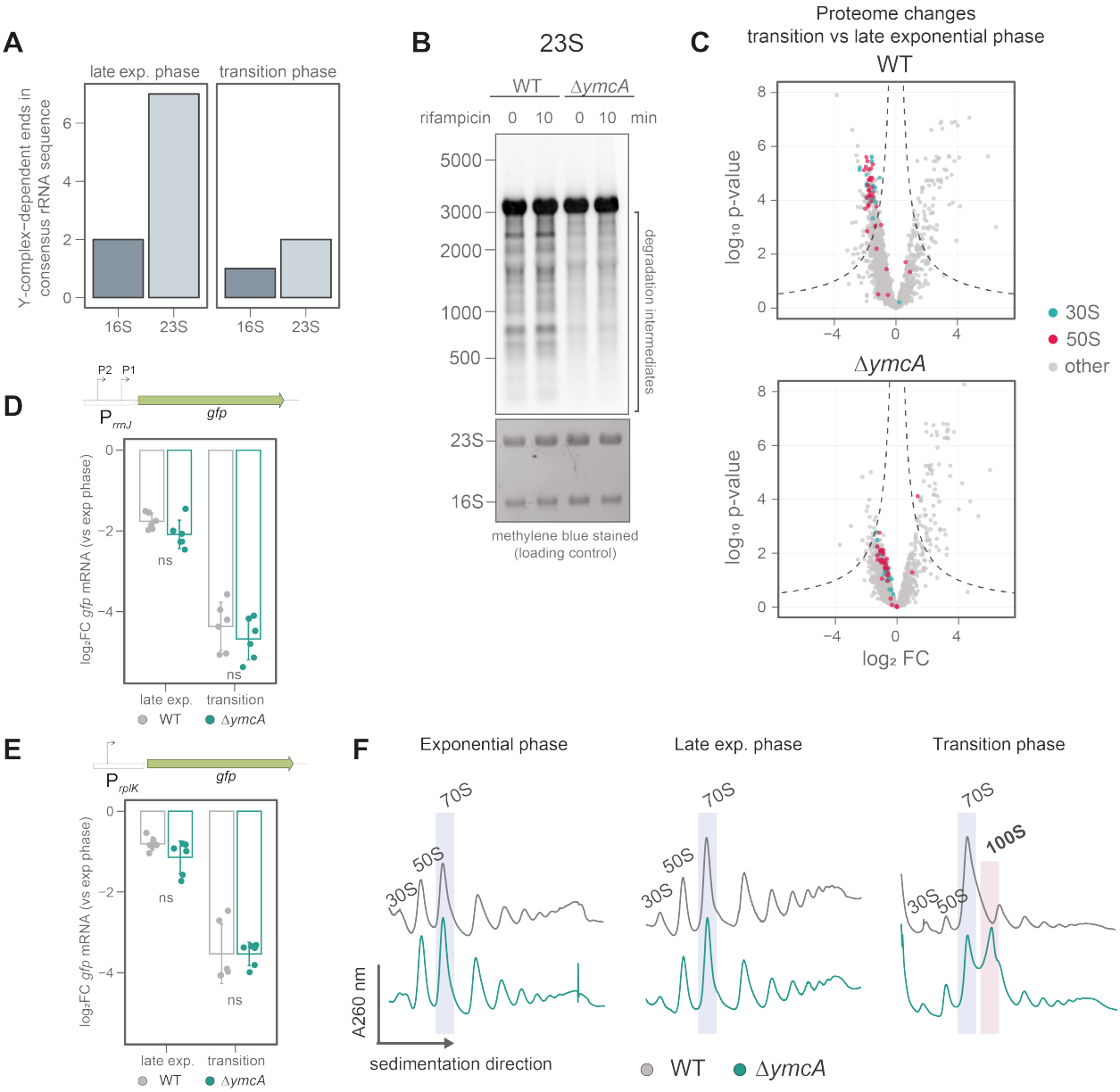

Figure 3. The Y-complex controls ribosome levels by initiating rRNA degradation. A) Number of cleavages detected by ISCP in *B. subtilis* rRNA during the late exponential and transition phase. **B)** Northern blot against 23S of WT and Δ*ymcA* cells at the late exponential phase, before and after treatment with 100 µg/ml rifampicin to stop transcription. The methylene blue-stained membrane is shown as a loading control. This image is representative of three biological replicates. **C)** Volcano plot of protein quantification of WT and Δ*ymcA* strains comparing transition to late exponential phase. The proteins composing the small (30S) and major (50S) ribosome subunits are highlighted in cyan and magenta, respectively. The data shows the average of four biological replicates. Activity of the promoter controlling **D)** *rrnJ* (rRNA) or **E)** the *rplK* (r-protein) transcription at late exponential and transition phase compared to the exponential phase in WT and Δ*ymcA*. The promoters were cloned controlling *gfp* transcription, which was measured using RT-qPCR. The *pcp* transcript was used as a reference. Individual values and the average ± standard deviation of three biological replicates and two technical replicates are shown. The statistical significance was tested using student's *t*-test. ns: *p*-value > 0.05. **F)** Ribosome sedimentation profile in 10-50% sucrose gradients of WT and Δ*ymcA* in exponential, late exponential, and transition phases. The 70S and 100S ribosomes are highlighted with a blue or red box, respectively. The data is representative of three biological replicates.

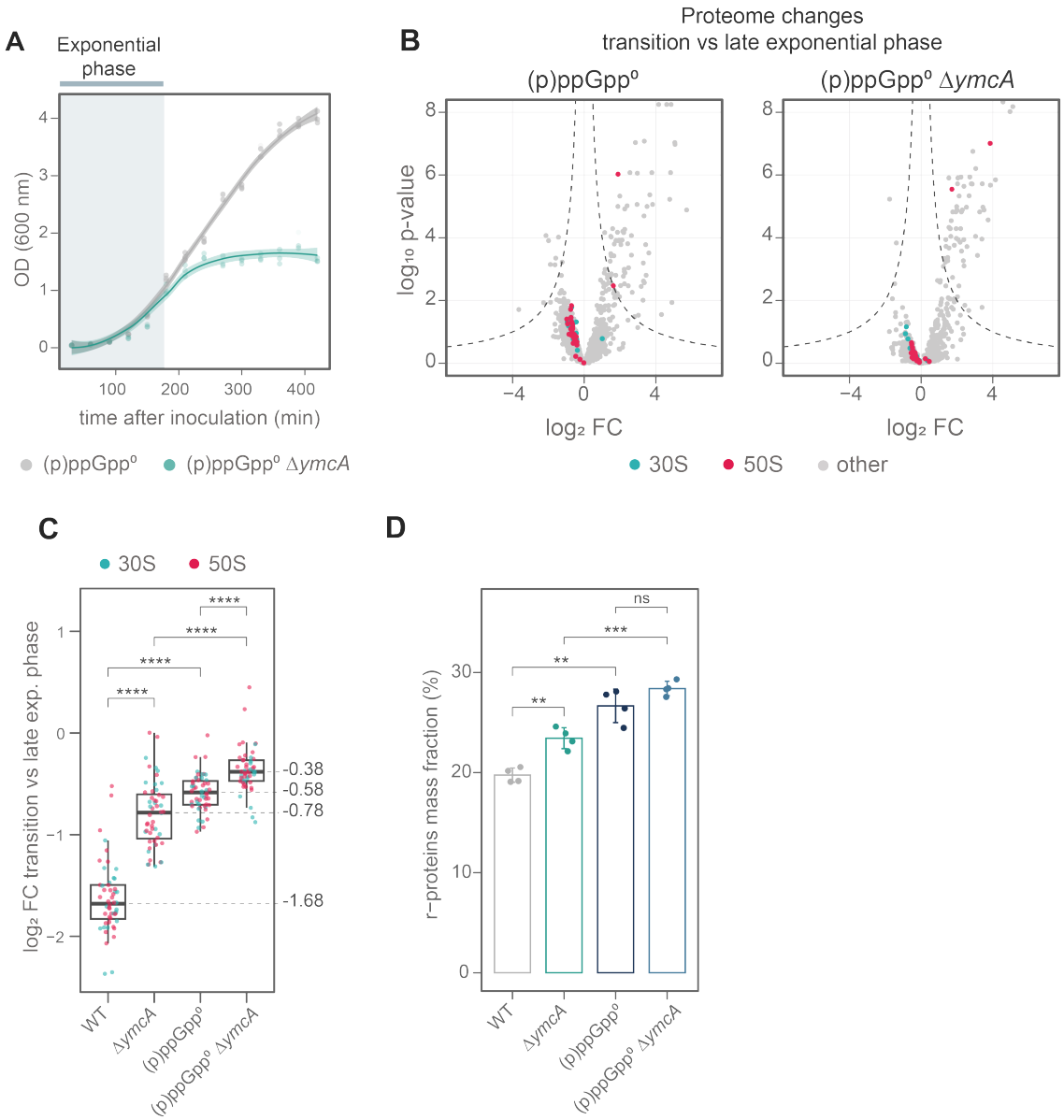

Figure 4. The alarmones (p)ppGpp and the Y-complex are important for controlling ribosome levels. A) Growth curve of (p)ppGpp^0 and (p)ppGpp^0 Δ*ymcA* strains in LB at 37°C. The blue bar marks the exponential phase. Three biological replicates are displayed with a smooth curve regression. **B)** Volcano plot of proteomic changes of (p)ppGpp^0 and (p)ppGpp^0 Δ*ymcA* cultures comparing transition to exponential phase. The proteins composing the small (30S) and major (50S) ribosome subunits are highlighted in cyan and magenta, respectively. The data shows the average of four biological replicates. **C)** Comparison of r-proteins downregulation in WT, Δ*ymcA,* (p)ppGpp^{0,} and (p)ppGpp^0 Δ*ymcA* during the transition phase compared to the late exponential phase. The boxplot represents the interquartile range (IQR) and the median in the center. Whiskers show the variability outside quartile 1 (Q1) and Q3 and were calculated as Q1-1.5*IQR and Q5+1.5*IQR, respectively. Proteins are highlighted like in **B**. Alternative r-proteins were excluded from the analysis. The statistical significance was tested using paired Wilcoxon test. ****: *p*-value ≤ 0.0001. **D)** Proteome fraction (in %) of r-proteins mass, measured by mass spectrometry. The r-protein mass fraction was calculated for the indicated strains. Individual values and the average ± standard deviation of three biological replicates are shown. The statistical significance was tested using student's *t*-test. ns: *p*-value > 0.05, **: *p*-value ≤ 0.01, ***: *p*-value ≤ 0.001.

759

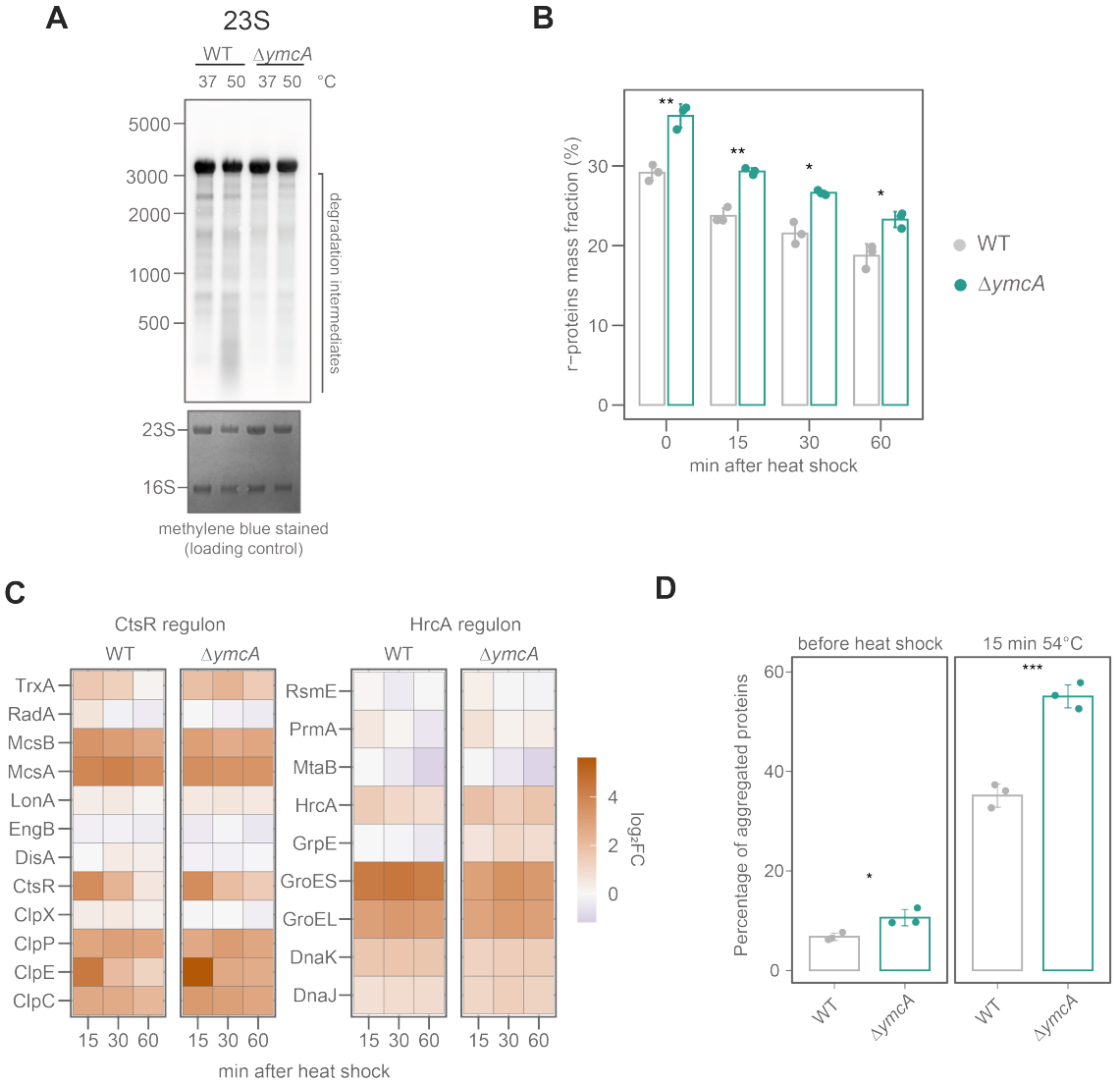

Figure 5. Control of ribosome levels and protein homeostasis in *ymcA* mutant during heat shock. **A)** Northern blot against 23S of WT and Δ*ymcA* cells at exponential phase before or after a heat shock. The methylene blue-stained membrane is shown as a loading control. This image is representative of three biological replicates. **B)** Proteome fraction (in %) of r-proteins mass, measured by mass spectrometry. Individual values and the average ± standard deviation of three biological replicates are shown. The statistical significance was tested using student's *t*-test. *: *p*-value ≤ 0.05, **: *p*-value ≤ 0.01. **C)** Induction of CtsR and HrcA regulons after heat shock (50°C) in WT and Δ*ymcA*. Proteins were measured by mass spectrometry. The color bar shows the $\log_2$ fold change compared to the control before heat shock. **D)** Percentage of aggregated proteins before and after a 15 min heat shock at 54°C in WT and Δ*ymcA*. Individual values and the average ± standard deviation of three biological replicates are shown. The statistical difference was tested using student's *t*-test. *: *p*-value ≤ 0.05, **: *p*-value ≤ 0.01, ***: *p*-value ≤ 0.001.

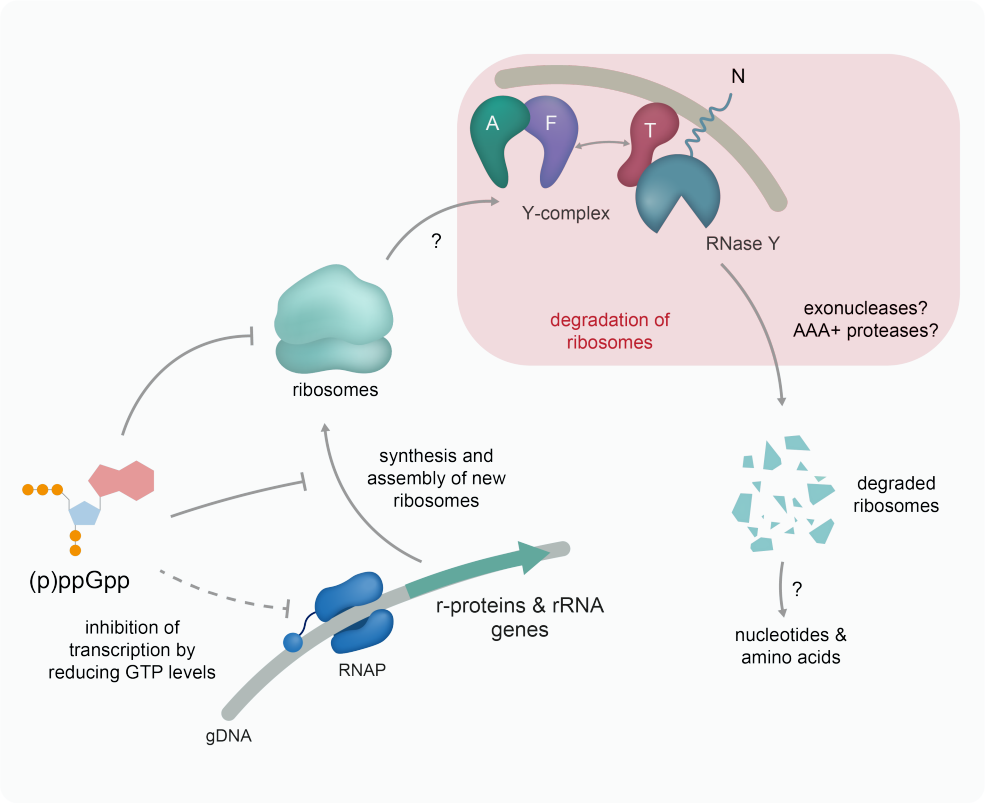

774

775 **Figure 6. Control of ribosome levels by (p)ppGpp and the Y-complex.** The alarmone (p)ppGpp
776 reduces the biogenesis of new ribosomes by indirectly inhibiting the transcription of rRNA and r-proteins
777 mRNA. (p)ppGpp inhibits GTPases that are involved in new ribosome assembly. Additionally, (p)ppGpp
778 reduces translation by binding to specific GTPases. The Y-complex can initiate the degradation of
779 ribosomes, which need to be transported to the membrane by unknown mechanisms. Exonucleases
780 and AAA+ protease complexes might assist in ribosome degradation for the complete degradation of
781 rRNA and r-proteins, which could partially replenish the nucleotide and amino acid pools during
782 starvation.

783

References

1. Hecker, M., Schumann, W. & Völker, U. Heat-shock and general stress response in *Bacillus subtilis*. *Mol. Microbiol.* **19**, 417–428 (1996).
2. Mogk, A. *et al.* The GroE chaperonin machine is a major modulator of the CIRCE heat shock regulon of *Bacillus subtilis*. *EMBO J.* **16**, 4579–4590 (1997).
3. Krüger, E. & Hecker, M. The first gene of the *Bacillus subtilis clpC* operon, *ctsR*, encodes a negative regulator of its own operon and other class III heat shock genes. *J. Bacteriol.* **180**, 6681–6688 (1998).
4. Elsholz, A. K. W., Michalik, S., Zühlke, D., Hecker, M. & Gerth, U. CtsR, the Gram-positive master regulator of protein quality control, feels the heat. *EMBO J.* **29**, 3621–3629 (2010).
5. Krüger, E., Witt, E., Ohlmeier, S., Hanschke, R. & Hecker, M. The Clp proteases of *Bacillus subtilis* are directly involved in degradation of misfolded proteins. *J. Bacteriol.* **182**, 3259–3265 (2000).
6. Alver, R. *et al.* The control of protein arginine phosphorylation facilitates proteostasis by an AAA+ chaperone protease system. Preprint at https://doi.org/10.1101/2022.09.15.508104 (2023).
7. Schäfer, H. *et al.* The alarmones (p)ppGpp are part of the heat shock response of *Bacillus subtilis*. *PLOS Genet.* **16**, e1008275 (2020).
8. Clay, K. J., Yang, Y., Clark, C. & Petrascheck, M. Proteostasis is differentially modulated by inhibition of translation initiation or elongation. *eLife* **12**, e76465 (2023).
9. Cherkasov, V. *et al.* Coordination of translational control and protein homeostasis during severe heat stress. *Curr. Biol.* **23**, 2452–2462 (2013).
10. Schramm, F. D., Schroeder, K. & Jonas, K. Protein aggregation in bacteria. *FEMS Microbiol. Rev.* **44**, 54–72 (2020).
11. Schäfer, H. *et al.* Spx, the central regulator of the heat and oxidative stress response in *B. subtilis*, can repress transcription of translation-related genes. *Mol. Microbiol.* mmi.14171 (2018).
12. Nakano, S., Erwin, K. N., Ralle, M. & Zuber, P. Redox-sensitive transcriptional control by a thiol/disulphide switch in the global regulator, Spx. *Mol. Microbiol.* **55**, 498–510 (2005).
13. Runde, S. *et al.* The role of thiol oxidative stress response in heat-induced protein aggregate formation during thermotolerance in *Bacillus subtilis*. *Mol. Microbiol.* **91**, 1036–1052 (2014).
14. Rochat, T. *et al.* Genome-wide identification of genes directly regulated by the pleiotropic transcription factor Spx in *Bacillus subtilis*. *Nucleic Acids Res.* **40**, 9571–9583 (2012).

819 15. Diez, S., Ryu, J., Caban, K., Gonzalez, R. L. & Dworkin, J. The alarmones (p)ppGpp
820 directly regulate translation initiation during entry into quiescence. *Proc. Natl. Acad. Sci.*
821 **117**, 15565–15572 (2020).
822 16. Corrigan, R. M., Bellows, L. E., Wood, A. & Gründling, A. ppGpp negatively impacts
823 ribosome assembly affecting growth and antimicrobial tolerance in Gram-positive
824 bacteria. *Proc. Natl. Acad. Sci.* **113**, (2016).
825 17. Pausch, P. *et al.* Structural basis for (p)ppGpp-mediated inhibition of the GTPase RbgA.
826 *J. Biol. Chem.* **293**, 19699–19709 (2018).
827 18. Krásný, L., Tišerová, H., Jonák, J., Rejman, D. & Šanderová, H. The identity of the
828 transcription +1 position is crucial for changes in gene expression in response to amino
829 acid starvation in *Bacillus subtilis*. *Mol. Microbiol.* **69**, 42–54 (2008).
830 19. Krásný, L. & Gourse, R. L. An alternative strategy for bacterial ribosome synthesis:
831 *Bacillus subtilis* rRNA transcription regulation. *EMBO J.* **23**, 4473–4483 (2004).
832 20. Koo, B.-M. *et al.* Construction and analysis of two genome-scale deletion libraries for
833 *Bacillus subtilis*. *Cell Syst.* **4**, 291-305.e7 (2017).
834 21. Msadek, T. *et al.* ClpP of *Bacillus subtilis* is required for competence development,
835 motility, degradative enzyme synthesis, growth at high temperature and sporulation. *Mol.*
836 *Microbiol.* **27**, 899–914 (1998).
837 22. Hajdusits, B. *et al.* McsB forms a gated kinase chamber to mark aberrant bacterial
838 proteins for degradation. *eLife* **10**, e63505 (2021).
839 23. Matavacas, J., Hallgren, J. & von Wachenfeldt, C. *Bacillus subtilis* forms twisted cells
840 with cell wall integrity defects upon removal of the molecular chaperones DnaK and
841 trigger factor. *Front. Microbiol.* **13**, (2023).
842 24. Schumann, W. Regulation of bacterial heat shock stimulons. *Cell Stress Chaperon.* **21**,
843 959–968 (2016).
844 25. DeLoughery, A., Dengler, V., Chai, Y. & Losick, R. Biofilm formation by *Bacillus subtilis*
845 requires an endoribonuclease-containing multisubunit complex that controls mRNA levels
846 for the matrix gene repressor SinR. *Mol. Microbiol.* **99**, 425–437 (2016).
847 26. DeLoughery, A., Lalanne, J.-B., Losick, R. & Li, G.-W. Maturation of polycistronic mRNAs
848 by the endoribonuclease RNase Y and its associated Y-complex in *Bacillus subtilis*. *Proc.*
849 *Natl. Acad. Sci.* **115**, E5585–E5594 (2018).
850 27. Broglia, L. *et al.* An RNA-seq based comparative approach reveals the transcriptome-
851 wide interplay between 3′-to-5′ exoRNases and RNase Y. *Nat. Commun.* **11**, 1587
852 (2020).
853 28. Taggart, J. C. *et al.* A high-resolution view of RNA endonuclease cleavage in *Bacillus*
854 *subtilis*. *Nucleic Acids Res.* **53**, gkaf030 (2025).

855 29. Khemici, V., Prados, J., Linder, P. & Redder, P. Decay-initiating endoribonucleolytic
856 cleavage by RNase Y is kept under tight control via sequence preference and sub-
857 cellular localisation. *PLOS Genet.* **11**, e1005577 (2015).
858 30. Le Scornet, A. *et al.* Critical factors for precise and efficient RNA cleavage by RNase Y in
859 *Staphylococcus aureus*. *PLOS Genet.* **20**, e1011349 (2024).
860 31. Shahbabian, K., Jamalli, A., Zig, L. & Putzer, H. RNase Y, a novel endoribonuclease,
861 initiates riboswitch turnover in *Bacillus subtilis*. *EMBO J.* **28**, 3523–3533 (2009).
862 32. Chao, Y. *et al.* In vivo cleavage map illuminates the central role of RNase E in coding
863 and non-coding RNA pathways. *Mol. Cell* **65**, 39–51 (2017).
864 33. Kime, L., Jourdan, S. S., Stead, J. A., Hidalgo-Sastre, A. & McDowall, K. J. Rapid
865 cleavage of RNA by RNase E in the absence of 5′ monophosphate stimulation. *Mol.*
866 *Microbiol.* **76**, 590–604 (2010).
867 34. Davis, J. H. & Williamson, J. R. Structure and dynamics of bacterial ribosome biogenesis.
868 *Philos. Trans. R. Soc. B Biol. Sci.* **372**, 20160181 (2017).
869 35. Piir, K., Paier, A., Liiv, A., Tenson, T. & Maiväli, Ü. Ribosome degradation in growing
870 bacteria. *EMBO Rep.* **12**, 458–462 (2011).
871 36. Eymann, C., Homuth, G., Scharf, C. & Hecker, M. *Bacillus subtilis* functional genomics:
872 global characterization of the stringent response by proteome and transcriptome
873 analysis. *J. Bacteriol.* **184**, 2500–2520 (2002).
874 37. Tagami, K. *et al.* Expression of a small (p)ppGpp synthetase, YwaC, in the (p)ppGpp^0
875 mutant of *Bacillus subtilis* triggers YvyD-dependent dimerization of ribosome.
876 *MicrobiologyOpen* **1**, 115–134 (2012).
877 38. Beckert, B. *et al.* Structure of the *Bacillus subtilis* hibernating 100S ribosome reveals the
878 basis for 70S dimerization. *EMBO J.* **36**, 2061–2072 (2017).
879 39. Carabetta, V. J. *et al.* A complex of YlbF, YmcA and YaaT regulates sporulation,
880 competence and biofilm formation by accelerating the phosphorylation of Spo0A: YmcA-
881 YlbF-YaaT complex stimulates the phosphorelay. *Mol. Microbiol.* **88**, 283–300 (2013).
882 40. Tortosa, P., Albano, M. & Dubnau, D. Characterization of *ylbF*, a new gene involved in
883 competence development and sporulation in *Bacillus subtilis*. *Mol. Microbiol.* **35**, 1110–
884 1119 (2000).
885 41. Branda, S. S. *et al.* Genes involved in formation of structured multicellular communities
886 by *Bacillus subtilis*. *J. Bacteriol.* **186**, 3970–3979 (2004).
887 42. Segev, E., Smith, Y. & Ben-Yehuda, S. RNA Dynamics in aging bacterial spores. *Cell*
888 **148**, 139–149 (2012).
889 43. Lehnik-Habrink, M. *et al.* RNase Y in *Bacillus subtilis*: a natively disordered protein that Is
890 the functional equivalent of RNase E from *Escherichia coli*. *J. Bacteriol.* **193**, 5431–5441
891 (2011).

892 44. Dubnau, E., DeSantis, M. & Dubnau, D. Formation of a stable RNase Y-RicT (YaaT)
893 complex requires RicA (YmcA) and RicF (YlbF). *mBio* e01269-23 (2023).
894 45. Hinrichs, R., Pozhydaieva, N., Höfer, K. & Graumann, P. L. Y-complex proteins show
895 RNA-dependent binding events at the cell membrane and distinct single-molecule
896 dynamics. *Cells* **11**, 933 (2022).
897 46. Lehnik-Habrink, M. *et al.* The RNA degradosome in *Bacillus subtilis*: identification of
898 CshA as the major RNA helicase in the multiprotein complex. *Mol. Microbiol.* **77**, 958–
899 971 (2010).
900 47. Commichau, F. M. *et al.* Novel activities of glycolytic enzymes in *Bacillus subtilis*. *Mol.*
901 *Cell. Proteomics* **8**, 1350–1360 (2009).
902 48. Durand, S. & Condon, C. RNases and Helicases in Gram-positive Bacteria. *Microbiol.*
903 *Spectr.* **6**, 10.1128/microbiolspec.rwr-0003–2017 (2018).
904 49. Kuroda, A. *et al.* Role of inorganic polyphosphate in promoting ribosomal protein
905 degradation by the Lon protease in *E. coli*. *Science* **293**, 705–708 (2001).
906 50. Dimitrova-Paternoga, L. *et al.* Structural basis of ribosomal 30S subunit degradation by
907 RNase R. *Nature* **626**, 1133–1140 (2024).
908 51. Boylan, S. A., Redfield, A. R., Brody, M. S. & Price, C. W. Stress-induced activation of
909 the sigma B transcription factor of *Bacillus subtilis*. *J. Bacteriol.* **175**, 7931–7937 (1993).
910 52. Njenga, R. K. *et al.* Ribosome-inactivation by a class of widely distributed C-tail anchored
911 membrane proteins. *Structure* **32**, 2259-2275.e6 (2024).
912 53. Wyant, G. A. *et al.* NUFIP1 is a ribosome receptor for starvation-induced ribophagy.
913 *Science* **360**, 751–758 (2018).
914 54. Gemin, O. *et al.* Ribosomes hibernate on mitochondria during cellular stress. *Nat.*
915 *Commun.* **15**, 8666 (2024).
916 55. Lehnik-Habrink, M. *et al.* RNA processing in *Bacillus subtilis*: identification of targets of
917 the essential RNase Y: Targets of the essential RNase Y in *Bacillus subtilis*. *Mol.*
918 *Microbiol.* **81**, 1459–1473 (2011).
919 56. Anderson, B. W., Fung, D. K. & Wang, J. D. Regulatory themes and variations by the
920 stress-signaling nucleotide alarmones (p)ppGpp in Bacteria. *Annu. Rev. Genet.* **55**, 115–
921 133 (2021).
922 57. Driller, K., Cornejo, F. A. & Turgay, K. (p)ppGpp – an important player during heat shock
923 response. *microLife* **4**, uqad017 (2023).
924 58. Benjamini, Y. & Hochberg, Y. Controlling the False Discovery Rate: A practical and
925 powerful approach to multiple testing. *J. R. Stat. Soc. Ser. B Methodol.* **57**, 289–300
926 (1995).
927 59. Lécrivain, A.-L. *et al.* In vivo 3′-to-5′ exoribonuclease targetomes of *Streptococcus*
928 *pyogenes*. *Proc. Natl. Acad. Sci.* **115**, 11814–11819 (2018).

929 60. Martin, M. Cutadapt removes adapter sequences from high-throughput sequencing
930 reads. *EMBnet.journal* **17**, 10 (2011).
931 61. Dobin, A. *et al.* STAR: ultrafast universal RNA-seq aligner. *Bioinformatics* **29**, 15–21
932 (2013).
933 62. Li, H. *et al.* The Sequence Alignment/Map format and SAMtools. *Bioinformatics* **25**,
934 2078–2079 (2009).
935 63. Smith, T., Heger, A. & Sudbery, I. UMI-tools: modeling sequencing errors in Unique
936 Molecular Identifiers to improve quantification accuracy. *Genome Res.* **27**, 491–499
937 (2017).
938 64. Liao, Y., Smyth, G. K. & Shi, W. featureCounts: an efficient general purpose program for
939 assigning sequence reads to genomic features. *Bioinformatics* **30**, 923–930 (2014).
940 65. Love, M. I., Huber, W. & Anders, S. Moderated estimation of fold change and dispersion
941 for RNA-seq data with DESeq2. *Genome Biol.* **15**, 550 (2014).
942 66. Putri, G. H., Anders, S., Pyl, P. T., Pimanda, J. E. & Zanini, F. Analysing high-throughput
943 sequencing data in Python with HTSeq 2.0. *Bioinformatics* **38**, 2943–2945 (2022).
944 67. Mölder, F. *et al.* Sustainable data analysis with Snakemake. Preprint at
945 https://doi.org/10.12688/f1000research.29032.2 (2021).
946 68. McCarthy, D. J., Chen, Y. & Smyth, G. K. Differential expression analysis of multifactor
947 RNA-Seq experiments with respect to biological variation. *Nucleic Acids Res.* **40**, 4288–
948 4297 (2012).
949 69. Geissler, A. S. *et al.* BSGatlas: a unified *Bacillus subtilis* genome and transcriptome
950 annotation atlas with enhanced information access. *Microb. Genomics* **7**, 000524 (2021).
951 70. Tareen, A. & Kinney, J. B. Logomaker: beautiful sequence logos in Python.
952 *Bioinformatics* **36**, 2272–2274 (2020).
953 71. Lorenz, R. *et al.* ViennaRNA Package 2.0. *Algorithms Mol. Biol.* **6**, 26 (2011).
954 72. Elfmann, C., Dumann, V., van den Berg, T. & Stülke, J. A new framework for SubtiWiki,
955 the database for the model organism *Bacillus subtilis*. *Nucleic Acids Res.* **53**, D864–
956 D870 (2025).
957 73. Pfaffl, M. W. A new mathematical model for relative quantification in real-time RT-PCR.
958 *Nucleic Acids Res.* **29**, 45e–445 (2001).
959 74. Hughes, C. S. *et al.* Single-pot, solid-phase-enhanced sample preparation for proteomics
960 experiments. *Nat. Protoc.* **14**, 68–85 (2019).
961 75. Kohler, D. *et al.* MSstats Version 4.0: Statistical analyses of quantitative Mass
962 Spectrometry-based proteomic experiments with chromatography-based quantification at
963 scale. *J. Proteome Res.* **22**, 1466–1482 (2023).
964 76. Jahn, M. *et al.* Growth of cyanobacteria is constrained by the abundance of light and
965 carbon assimilation proteins. *Cell Rep.* **25**, 478-486.e8 (2018).

966 77. Jahn, M. *et al.* Protein allocation and utilization in the versatile chemolithoautotroph
967 *Cupriavidus necator*. *eLife* **10**, e69019 (2021).
968